DØ TOP RESULTS, QCD, ELECTROWEAK, AND NEW PHENOMENA PHYSICS AT FERMILAB

Maris Abolins*
Department of Physics and Astronomy
Michigan State University
East Lansing, MI 48824

For the DØ Collaboration

ABSTRACT

This paper reviews physics at the Fermilab proton-antiproton collider. Included are results from the 1992–93 run, giving the DØ top cross section limits and selected topics from both DØ and CDF in the areas of QCD, electroweak and new phenomena physics.

*Supported by the National Science Foundation under Grant PHY93-19216.

1 Introduction

In this talk, I will review some physics results that have come out of the 1992-93 run (Run IA) at the Fermilab proton-antiproton collider. I will discuss selected topics in the areas of QCD, electroweak physics, and the search for new phenomena by both DØ and CDF collaborations, and I will end with a discussion of the DØ search for the top quark.

2 QCD Physics at CDF and DØ

A. Overview

The topics within QCD are many and varied, and some selection must be made because of time limitations. I will focus on four areas where there has been recent progress or some new results have come out: Energy Flow in Jets, Single-Jet Inclusive Cross Section, Direct Photon Production, and Rapidity Gaps.

B. Energy Flow in Jets

1. Method of Analysis

We wish to study how the energy distribution within a jet cone depends on external variables such as the jet's transverse energy, ET and rapidity, h, and to see how well our measurements agree with the predictions of specific models and calculations. To do this we define a function f(R) in Figure 1:

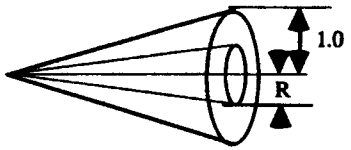

$$f(R) = \frac{\int_{0.0}^{R} E_t(r)dr}{\int_{0.0}^{1.0} E_t(r)dr}.$$

Figure 1: Definition of function f(R).

This function measures the transverse energy distribution within a jet. A rapid rise at low R indicates a narrow jet whereas a wide jet is characterized by a slower increase.

2. Selection of Data Sample

Standard jet quality cuts are imposed to remove hot cells and energy deposited from main ring backgrounds. The vertex position is required to be $|z| < 30$ cm to ensure that calorimeter towers remain projective. Corrections are applied to remove E_T contributions from the underlying event[1] and the effects of uranium noise.[2] For purposes of this analysis, the data are subdivided into two regions in η, a central region with $|\eta| < 0.2$ and a forward region with $2.5 < |\eta| < 3.0$ and four E_T ranges: 45 – 70, 70 – 105, 105 – 140, and > 140 GeV.

In Figure 2, I show a plot of f(R) for central events with $|\eta| < 0.2$ for the four ranges in E_T. The general trend of the data is clear: higher transverse energy jets appear to be narrower.

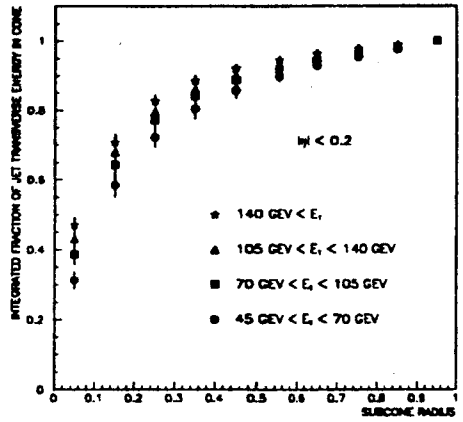

Figure 2: Jet cone energy distribution for central events.

3. Comparison at Particle Level

For clarity, we would like to make the comparison at the "particle" level before showering and possible calorimeter effects obscure the underlying physics. Two effects can possibly affect our results: non-uniform calorimeter response which would tend to make jets narrower, and the effects of showering which would artificially broaden the jet. We use the detector simulator program GEANT[3] to estimate the effects of the calorimeter. To gauge the effects of varying fragmentation, we tried three different Monte Carlo generation

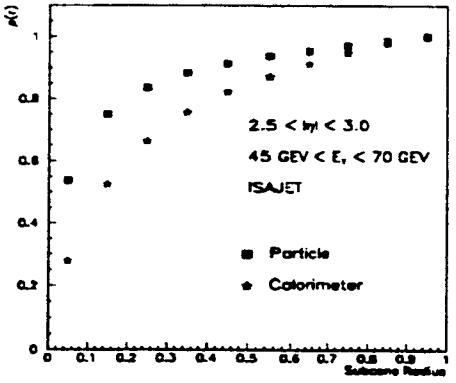

Figure 3: Effect of corrections in forward direction.

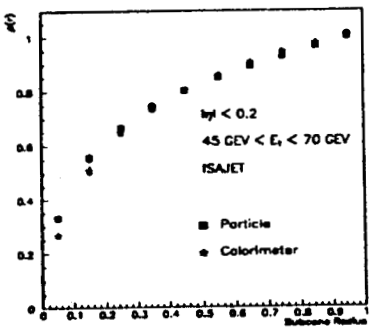

Figure 4: Central corrections.

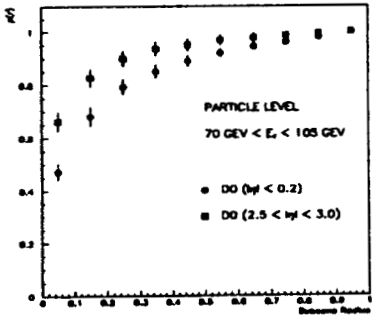

Figure 5: Particle level comparison.

programs: Isajet,[4] Herwig,[5] and Pythia.[6] The dominant effect was due to showering with corrections of 7% in the central region and as high as 30% in the forward. Figure 3 shows the narrowing of the jets at the particle level in the forward region and Figure 4 the smaller effect in the central region. We should note that the ideal comparison would be at parton level, which is inaccessible to us. Going to particle level does remove the gross effects of the calorimeter.

A comparison of forward and central jets, corrected to particle level, in Figure 5 shows clearly that forward jets tend to be narrower at fixed E_T than central.

Work is underway to see if this asymmetry is due to the fact that there are more gluon jets produced in the central region than in the forward.

4. Comparison with Theory

It would be instructive as well as useful if the results could be predicted in detail by some QCD-based model. We have used the program JETRAD[7] which uses next-to-leading order loops as well as diagrams at tree level to make predictions of jet shapes. It is important to bear in mind that the predictions are at the parton level and our data is corrected back to the particle level only. Figure 6 shows a comparison of our particle level data with JETRAD predictions at three different renormalization scales for central jets with 105 GeV < E_T < 140 GeV, and Figure 7 is a comparison for forward jets with 45 GeV < E_T < 70 .

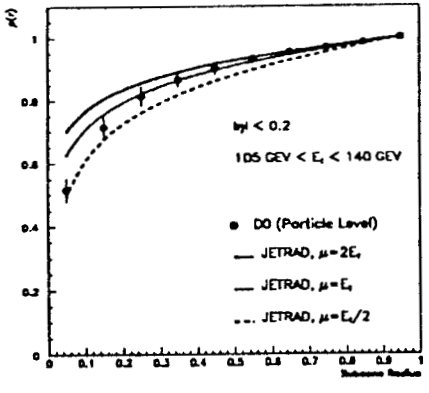

Figure 6: Comparison with JETRAD for central jets.

Although agreement is best at a scale of $\mu = E_T$, no choice of scale gives good agreement for all values of subcone radius, and the disagreement is worse in the forward direction than the central.

5. Summary of Results

We have a number of basic conclusions:

- Jets get narrower with increasing E_T. This is expected if particle momentum transverse to the jet axis remains constant.
- Forward jets are narrower than central jets. If quark jets, which are expected to be narrower, dominate the forward direction, then this would be a good explanation. Work is underway to verify this.
- Many of the popular jet Monte Carlos do a good job of predicting jet shapes, particularly in the central region. This includes Herwig, Pythia, and Isajet. The program JETRAD does not do very well no matter what the choice of scale.

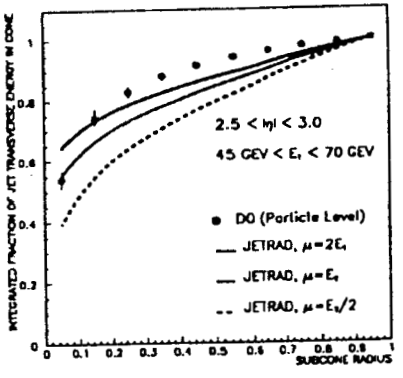

Figure 7: Comparison with JETRAD for forward jets.

6. Future Plans

Work is underway to understand the differences of quark and gluon jets in DØ and possibly devise tags for use in other applications.[8]

C. Single-Jet Inclusive Cross Section

1. Rationale

Single-jet inclusive cross sections have been available from CDF[9] out to $|\eta|<0.7$ for some time. In this talk, I present preliminary measurements from DØ covering a range of pseudorapidity $|\eta|< 3.0$. This is of interest as previous measurements at UA2[10] did not show good agreement with theory at large values of $|\eta|$, and this is the first opportunity to see if this disagreement persists at Tevatron energies.

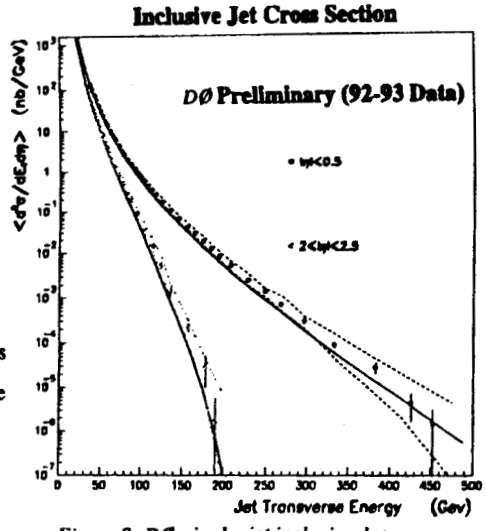

Figure 8: DØ single-jet inclusive data.

2. DØ Data

The DØ data have the resolution unfolded and use a cone size of $\Delta R = 0.7$ in the usual η, ϕ space. Figure 8 and Figure 10 summarize the results for four separate ranges in η. The predictions of theory are given by the solid line and the dashed bands indicate the range of variation in the data introduced by uncertainties in the energy scale. Good agreement is obtained at this level of precision.

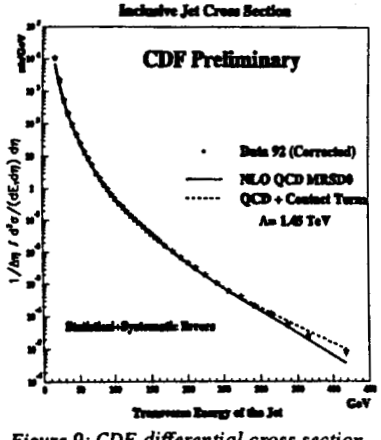

Figure 9: CDF differential cross section with theory curve superimposed.

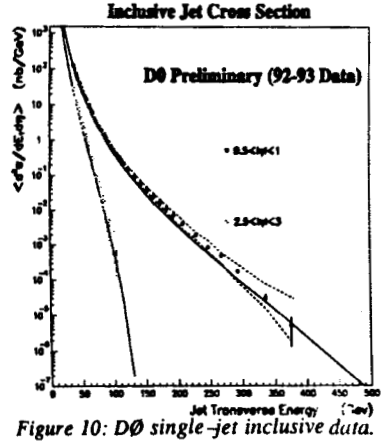

Figure 10: DØ single-jet inclusive data.

3. CDF Data

Figure 9 shows the CDF double-differential cross section as a function of transverse energy for jets with $|\eta| < 0.7$.

The data, which has been corrected for resolution, is indistinguishable from predictions of NLO QCD based on MRSDØ structure functions. Plotted also is the QCD prediction with the addition of a contact term with a compositeness scale of 1.45 TeV. The sensitivity to quark compositeness is better indicated in Figure 11 which shows a ratio of data to theory for various choices of the compositeness scale. Figure 12 shows the CDF single-jet inclusive data in a comparison with theory. Note that the agreement is generally good with some deviations at the lowest and highest transverse energies.

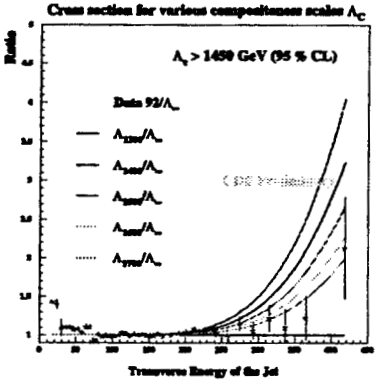

Figure 11: Compositeness scale effect.

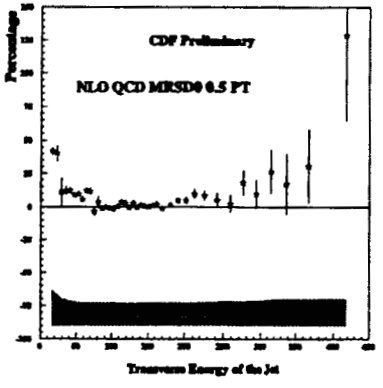

Figure 12: CDF Data-Theory for $|\eta|<0.7$

4. Principal Conclusions

a) CDF

- the compositeness limit $\Lambda_C > 1450$ GeV,

- uncertainties in the data are now sufficiently small to constrain parton distributions , and
- agreement with theory (and DØ) is excellent.

b) DØ

- single-jet cross section is in reasonable agreement with NLO QCD. This covers a range in $|\eta|$ where disagreement existed at lower energies , and
- work is in progress on setting limits on quark compositeness.

D. Direct Photon Production

1. Motivation

At low E_T the process is expected to be dominated by QCD-Compton scattering (Figure 13) and is thus sensitive to the gluon content of the hadron. It could also give a good measure of the charm content of the proton if a c quark is detected along with the photon. The measurement is made difficult because of the large backgrounds of π^0's and η's which obscure the single-photon signal.

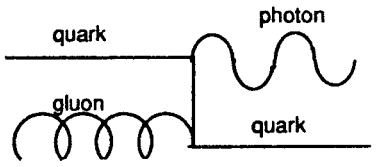

Figure 13: Tree level gluon diagram.

2. Strategies for Extracting the Signal

Both CDF and DØ use similar strategies for selecting the single-photon candidate events. An isolation criterion is imposed, limits are placed on missing transverse energy, and the event is rejected if there is an associated charged track. Both analyses rely on converting the photon in material in the detector and then analyzing the resulting shower. In DØ, the conversion takes place either in the central drift chambers or the first layer of the calorimeter (EM-1). The photon is then identified by its transverse profile in EM-3, the layer of the calorimeter with the best spatial resolution. In CDF, two methods are used: if the conversion takes place in the solenoid magnet material, the resulting pairs are measured. Otherwise, the transverse profile of the shower is measured in the electromagnetic calorimeter, CES.

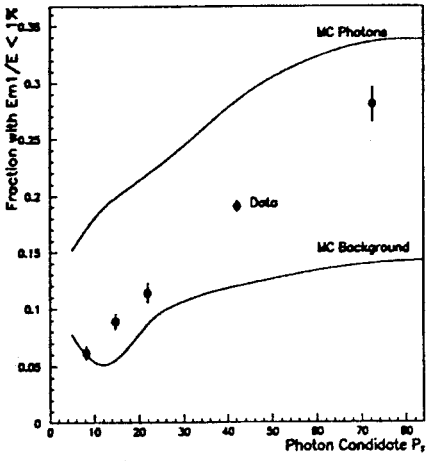

Figure 14: Data and Monte Carlo for DØ with no showering in EM-1.

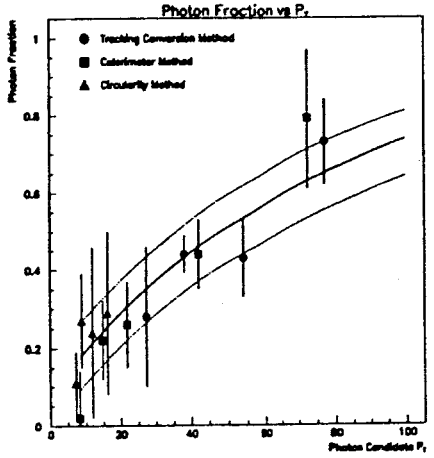

Figure 15: Photon fractions in DØ using three different methods.

Figure 14 shows the DØ data with no showering in the first layer of the electromagnetic calorimeter (EM1) plotted as a function of the photon transverse momentum. The two curves are Monte Carlo estimates from real photons and from QCD background. Figure 15 shows the photon fraction as a function of its transverse momentum, extracted using conversions in tracking chambers, conversions in the calorimeter, and from a shape analysis in EM-3. The dashed lines represent the uncertainties in the central value (solid line).

The resulting DØ photon cross section and comparison to theory are shown in Figure 16. Both systematic and statistical error bars are shown. The trend of the data is to follow the theory even though some deviation could be accommodated by the large error bars.

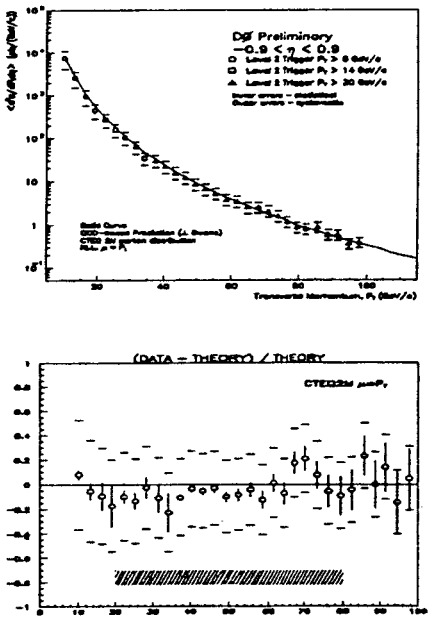

Figure 16: DØ data and fractional deviation from theory.

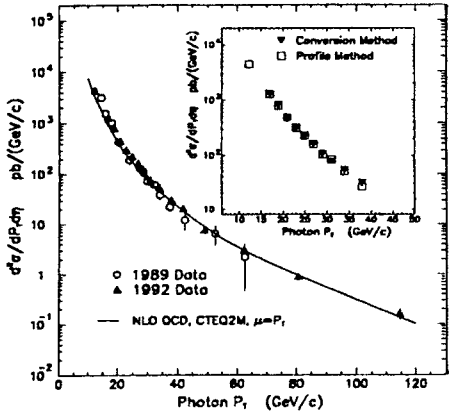

Figure 17: CDF cross section data.

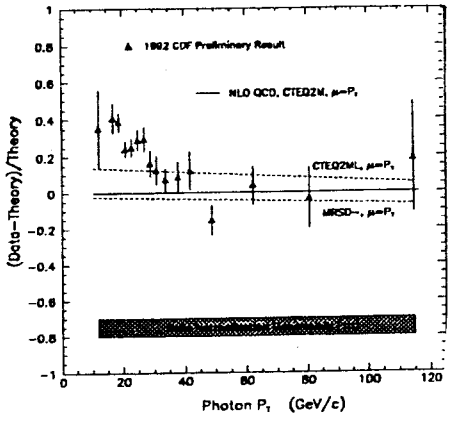

Figure 18: CDF fractional deviation.

The corresponding CDF data are shown in Figure 17. The data are of high quality and show a clear departure from theory for momenta of less than about 30 GeV/c. This is made clear when the fractional difference of data to theory is plotted as in Figure 18.

3. Principal Conclusions

- DØ results are in good agreement with QCD-based predictions in the range of 10–100 GeV.
- The CDF higher precision measurement departs from predictions at E_T below about 30 GeV. This could be due to problems with the structure functions used or possibly a result of final or initial quark bremsstrahlung which has been incompletely treated.
- Although the DØ data does not show the rising trend at low E_T indicated by the CDF result, the systematic error bars are large enough to accommodate such an effect.

E. Rapidity Gaps

1. Introduction

Rapidity gaps in collisions were first observed by Cocconi[11] in cosmic rays. Much subsequent theoretical and experimental work led to the ideas of diffraction dissociation[12] and Pomeron exchange as explanations for this phenomenon. An analysis using the modern language of colorless exchange was initially presented by Dokshitzer, Khoze, and collaborators,[13] but it lay neglected until it was revived by Bjorken[14] who pointed out its importance at high-energy colliders. Schematically, a gap along with a pair of jets is shown in Figure 19.

The experimental challenge is to find such events in the presence of backgrounds that can statistically fake this phenomenon. In a lowest order QCD calculation, Bjorken estimated the ratio of "gap" to conventional gluon-exchange events with the same jet kinematics to be about 0.1. This can be expressed as:

$$f = \frac{\sigma_{gap}}{\sigma} \cdot S. \qquad (1)$$

In this expression, the ratio of the gap to total cross section is multiplied by a factor "S" for the survival probability of the gap in the presence of spectator interactions.

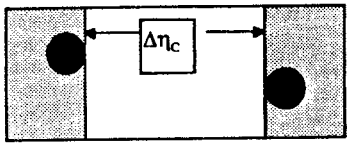

Figure 19: Schematic of dijet and rapidity gap.

2. DØ Results

In the DØ experiment, rapidity gaps are sought by counting the number of EM towers with transverse energy greater than 200 MeV. Possible evidence for gaps can be seen in Figure 20, which shows a multiplicity distribution of such towers for $\Delta\eta_C > 3$. A quantitative analysis of the data is performed by fitting these multiplicity distributions to negative binomial distributions and determining the excess at low multiplicity. The difference of the fit and the data is shown in Figure 21 where this excess is plotted vs. $\Delta\eta_C$. This excess is interpreted as evidence for rapidity gaps in the DØ experiment.

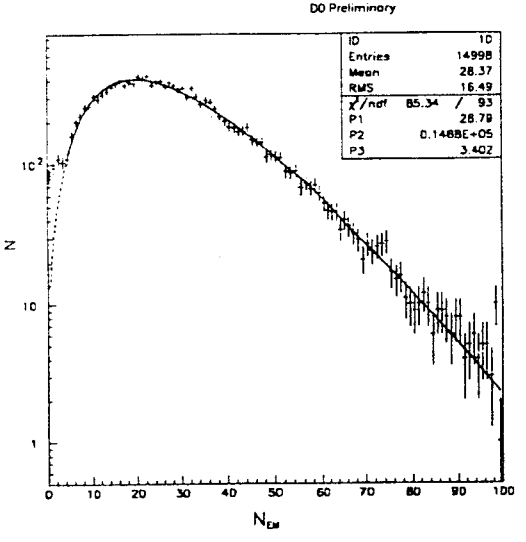

Figure 20: Multiplicity distribution of towers with energy.

Numerically, the fit yields for the excess fraction of events with no energy between jets in the range $\Delta\eta_c > 3.0$:

$f = 1.4 \pm 0.2 \pm 0.2 \times 10^{-2}$,

where the first uncertainty is statistical, and the second, systematic due to the fitting procedure.

The excess cannot be explained by detector effects. It is not there in Monte Carlo studies and does not appear in a control sample of three-jet events, where the third jet is removed. The effect is consistent with that expected from color singlet exchange.

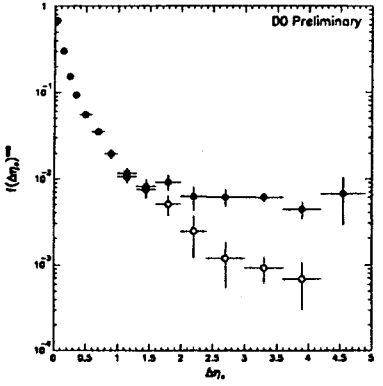

Figure 21: Measured and predicted distributions.

3. CDF Results

A recent CDF analysis of data from 1988-89 shows evidence for the existence of rapidity gaps. Their technique differs from DØ in that they attempt to identify gaps by counting charged tracks in rapidity intervals and not energy deposition in calorimeters. Events are chosen with at least one energy cluster exceeding 60 GeV, and then, the frequency of tracks is examined as a function of the rapidity gap between the two leading jets. This fraction is shown in Figure 22. The flattening of the curve represents an irreducible fraction of events with zero tracks and thus a rapidity gap. As in DØ, the fraction of rapidity gap events is extracted by fitting negative binomial distributions to the track multiplicity distributions as a function of η.

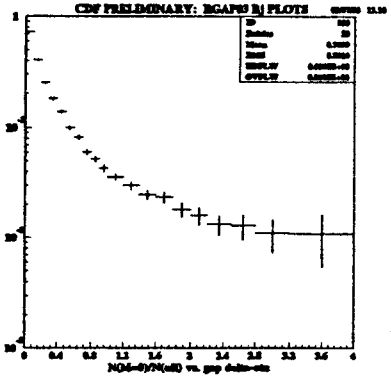

Figure 22: CDF background subtracted zero-multiplicity events.

Comparison is made to a control region where no gap is expected.

The results are summarized in Figure 23 which shows a clear excess of events in the signal region. No comparable signal is seen in the control region. The excess is at the level of 0.0086 ± 0.0012 (statistical) +0.0024 - 0.0012 (systematic).

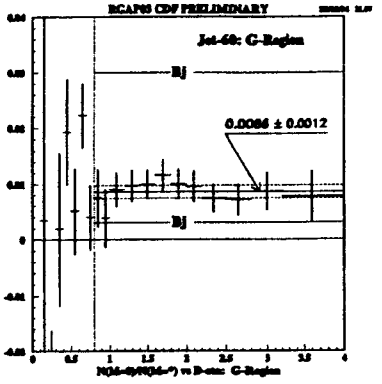

Figure 23: Fraction of zero track events in the signal region.

3 New Physics

A. Search for Leptoquarks

Leptoquarks are hypothesized objects that couple to leptons and quarks within a given generation. Both DØ and CDF have produced analyses based on integrated luminosities of 13.4 and 19.7 pb^{-1}, respectively, that place new lower limits on the masses of these particles. Figure 24 shows the DØ 95% confidence limits on first generation leptoquarks. Plotted is a curve of branching fraction into an electron vs. mass of the leptoquark. The limit from this analysis is 130(116) GeV if the branching fraction is 100(50%).

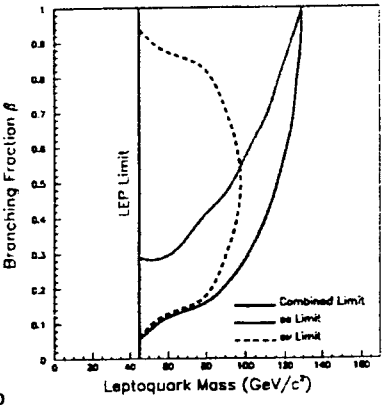

Figure 24: DØ limits on first generation leptoquarks.

The corresponding DØ analysis results on the search for second generation leptoquarks are shown in Figure 25 along with the earlier limits from LEP. The analysis yields limits of 97.5 GeV and 80 GeV for the same two choices of couplings at a 95% confidence level. The searches look for a high P_T muon plus a dijet. The CDF second generation analysis actually results in two candidate events which are consistent with a calculated background of 1.35±0.50 events. Their limits for the two choices of branching fractions are 133 and 98 GeV/c^2 respectively.

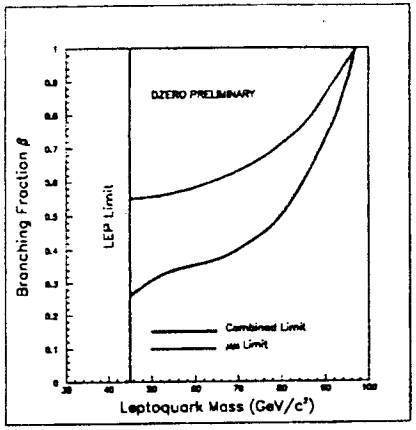

Figure 25: DØ second generation leptoquark limits.

B. Supersymmetry Searches

Another active area of new particle searches is the quest for the supersymmetric partners of the known fermions and bosons. The current situation summarizing the limits set by the LEP experiments and recent results from DØ and CDF is shown in Figure 26,where the limits are shown on a plot of mass of squark vs. the mass of the gluino. As indications of the sensitivity of the search,we quote the DØ 90% confidence level limits for two assumptions about the mass of the squark:

- If m(squark) --> infinity, m(gluino)>146 GeV.
- If m(squark) = m(gluino), m(gluino)>205 GeV.

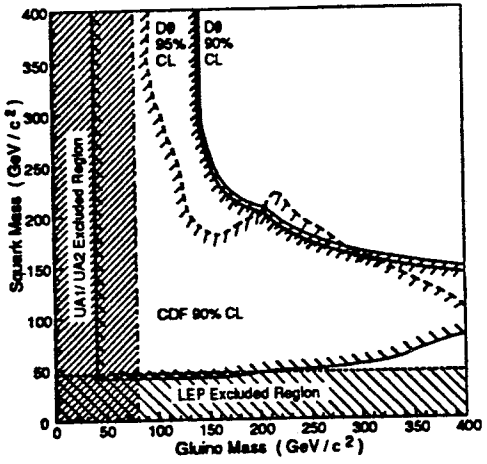

Figure 26: Gluino mass limits.

4 Electroweak Physics

A. W Mass Measurement

1. Introduction

A precision measurement of the W boson mass (M_W) in combination with measurements from e^+e^- colliders at the Z^0 pole places strong constraints on the parameters of the Standard Model (SM). Among these are the masses of the top quark and the Higgs boson which appear in loop corrections to the SM and renormalize M_W. While the dependence on the Higgs is only logarithmic, for the top quark it is quadratic.

2. Method and Experimental Considerations

The mass measurement of the W boson, in both CDF and DØ, is extracted from the leptonic spectra of its decays into a lepton and its associated neutrino. In the CDF experiment,both electron and muon decays are used whereas DØ uses only electrons. Longitudinal energy losses in the detectors preclude a true effective mass measurement, and one has to be content with measuring the transverse mass, defined by:

$$M_T^2 = 2P_T^l P_T^V \cdot (1 - \cos\phi_{lV}) \,, \qquad (2)$$

where $P_T^\nu = -P_T^l - P_T^{recoil}$ is the missing transverse momentum. The information on the W mass is contained in the high mass edge of the transverse mass distribution. Its precise determination is complicated by experimental resolution and other detector-dependent effects. On the positive side, the cross section is large (~2 nb),which yields many thousands of events even after stringent cuts on the data.

The mass is extracted from a likelihood fit to the transverse mass distribution with all detector effects modeled and the mass itself left as a parameter to be determined. The critical issues in this analysis are:

- the lepton-energy scale ,
- the lepton-energy resolution ,
- the hadronic-energy response , and
- various production-model assumptions.

The lepton energy scale in DØ is determined in two, complementary ways. First, $Z^0 \rightarrow e^+e^-$ events, constrained to the Z^0 mass, provide a sample of calibration electrons with E_T's near those arising from W decays. This calibration is statistically limited and currently gives an uncertainty of 310 MeV. The second method anchors the scale on two resonant states, the Z^0 and J/ψ, found in the experiment. This method gives an uncertainty in the mass of the W of less than 200 MeV and is also dominated by the statistical uncertainty in the Z^0 sample. The larger value is used in the current analysis.

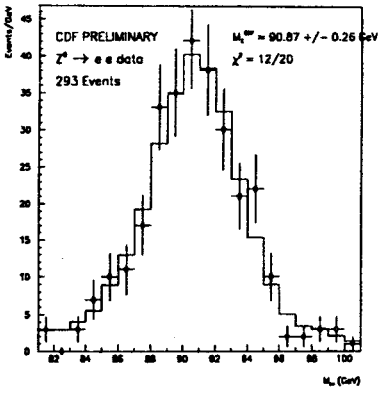

Figure 27: CDF Z --> ee data.

CDF uses its central magnetic field and excellent tracking to fix their energy scale for muons on the Z^0 as well as the ψ/J and Υ. The resulting massuncertainty of the W is 130 MeV. For electrons, the calibration procedures and resulting uncertainties are similar for the two experiments.

Two issues are important for a measurement of the missing transverse momentum: the hadronic energy scale already mentioned and the effect of the underlying event. The two experiments take slightly different approaches to address this problem. In CDF, the underlying event is taken from spectator events and the hadronic energy scale is derived from Z^0 data, where the Z^0 is assumed to have identical production properties to the W. In the DØ experiment, the effect of the underlying event is extracted using a W Monte Carlo in association with a library of minimum bias events collected over a range of instantaneous luminosities.

Studies of the hadronic activity accompanying $Z^0 \rightarrow e^+e^-$ events suggest that the simulated events should have added to them 1.1 times the average E_T of the minimum bias events at the same luminosity. The hadronic energy scale is then relative to the electron scale with Z^0 events by balancing the transverse momentum of the electromagnetically decaying Z^0 relative to the hadronic recoil. The effects of the electron resolution is minimized by the appropriate choice of projections of the measured transverse momentum components. The resulting comparison of Monte Carlo and data is good in all kinematical quantities. Ultimately, the electron energy scale is determined from a Z^0 mass measurement with the calorimeter that is calibrated to the precision results from the LEP experiments.

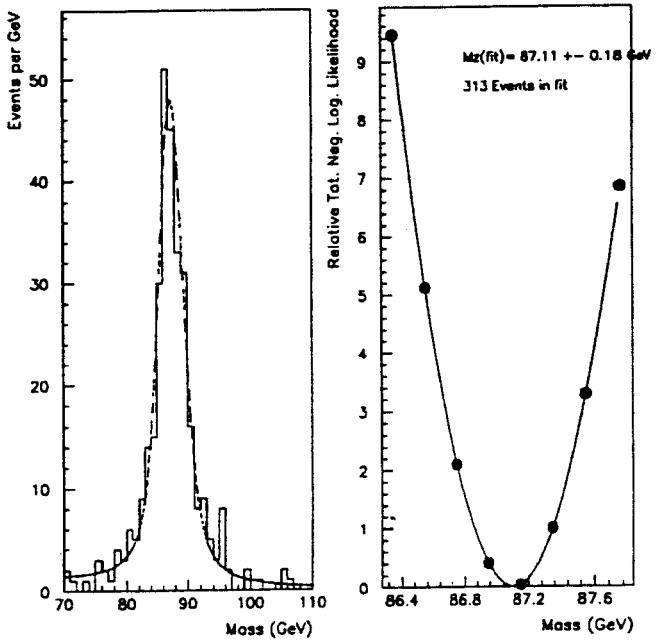

Figure 28: DØ Z--> ee data and mass fit.

The $Z^0 \rightarrow e^+e^-$ mass spectrum from CDF is shown in Figure 27, and the corresponding mass plot for DØ along with the χ^2 plot from a mass fit in Figure 28. By virtue of their central magnetic field, CDF is also able to get a high precision measurement of $Z^0 \rightarrow \mu^+\mu^-$.

3. Results

The CDF transverse mass spectrum for W --> e ν is shown in Figure 29 and that for DØ in Figure 30. Not shown is the CDF data of W--> μ ν, which is of comparable quality. Table 1 summarizes the parameters of the fits. Shown are columns of data type, number of events, the W mass, statistical error, systematic error, scale error for DØ, and the result of combining these errors in quadrature. The last row shows the best estimate of the W mass and error with the older UA2 data added. In making the combined result, correlated errors were properly treated.

Table 1: W mass values and uncertainties.

Data	# events	M_W	Stat	Syst	Scale	Combined
DØ	5830	79.86	0.16	0.16	0.26	0.345
CDF(eν)	6421	80.47	0.15	0.25		
CDF(μν)	4090	80.29	0.20	0.24		0.23
CDF, DØ UA-2		80.23				0.18

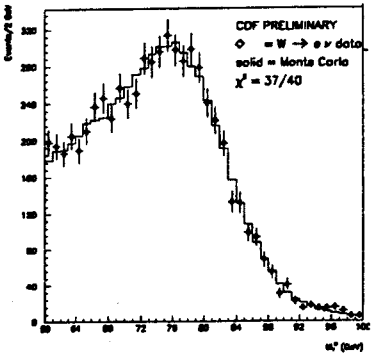

Figure 29: CDF W transverse mass.

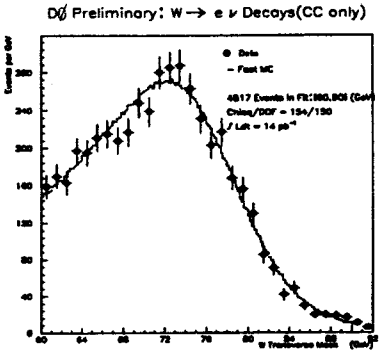

Figure 30: DØ W--> e ν transverse mass.

The data in Table 1 is displayed graphically in Figure 32 where the predictions from LEP Z^0 pole measurements are shown as a band and the SLAC asymmetry prediction is given by the solid line with dotted lines indicating one standard deviation uncertainties.

A detailed analysis of the mass uncertainties for DØ and CDF, shown in Figure 31, indicates that the largest contributions are statistical followed by systematic effects due to resolution and the uncertainties associated with the hadronic energy scale. DØ includes a separate contribution from uncertainties in the overall electron energy scale, while CDF includes a scale uncertainty in quadrature with all other systematic uncertainties. All of these effects will be decreased with increased running since the scale uncertainties are effectively addressed by detailed calibration of the detector with Z^0's. There are also prospects for decreasing the scale error in the DØ measurement by anchoring it firmly at the low end on π^0's and J/Ψ, and Υ electromagnetic decays. Ultimate mass uncertainties in the 50–100 MeV/c^2 range are expected, promising an interesting confrontation with the indirect measurements of the W mass, and hence, with the Standard Model. The connection of this measurement to the top quark and Higgs is shown in Figure 33, where the mass of the top quark is plotted against M_W along with

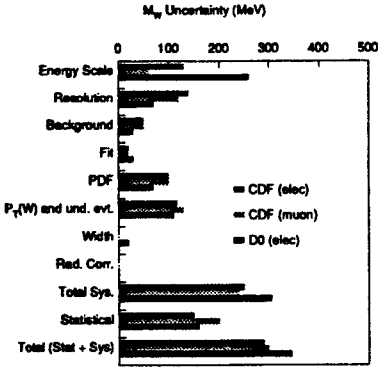

Figure 31: W mass uncertainties.

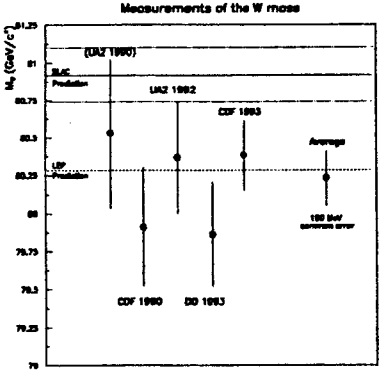

Figure 32: W mass measurements.

the world average measurement, the predictions from LEP and from SLC. The direct measurements are in good agreement with LEP predictions and favor a top mass in the range recently reported.[15] The SLC measurement favors a larger top mass but the discrepancy is less than 3 σ. This situation should be clarified during the next several years when additional data from SLD becomes available.

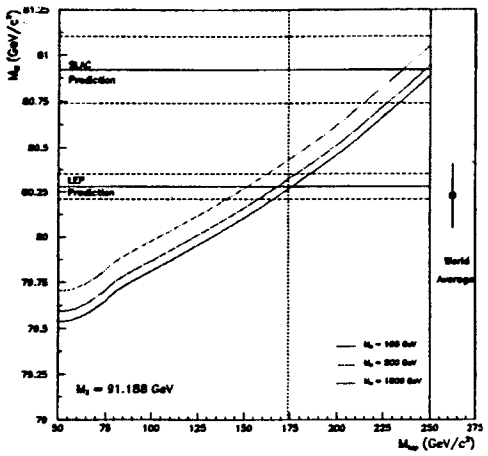

Figure 33: W mass as a function of top mass.

B. Production of Vector Boson Pairs

1. Introduction

With Lorentz invariance as the only constraint, 14 parameters are necessary to completely specify the WWγ and WWZ coupling constants. In the Standard Model, all triboson couplings are completely specified, but there are nonstandard models, such as those with composite vector bosons, that have anomalous couplings which modify the static properties of the bosons and have predictable effects on their production rates and kinematic distributions. A class of such models that satisfy gauge invariance for photons and do not permit CP violation can be characterized by nonzero values for two parameters, commonly referred to as $\Delta\kappa$ and λ. Among other effects, they modify the magnetic moment of the W:

$$\mu_W = \frac{e}{2m_W}(2+\Delta\kappa+\lambda) \qquad (3)$$

and change the production cross section for vector boson pairs:

$$\sigma \propto \left[c_1\lambda^2 + c_2\Delta\kappa^2\right]. \qquad (4)$$

In order not to violate unitarity at high energy, form factors have to be introduced in the anomalous couplings:

$$\lambda(\hat{s}) = \lambda_0\left(1+\frac{\hat{s}}{\Lambda^2}\right)^n. \qquad (5)$$

In experiments at the Fermilab collider, we look for evidence for anomalous couplings in changed production rates or kinematic properties for events containing Wγ, Zγ, WW, WZ, or ZZ bosons.

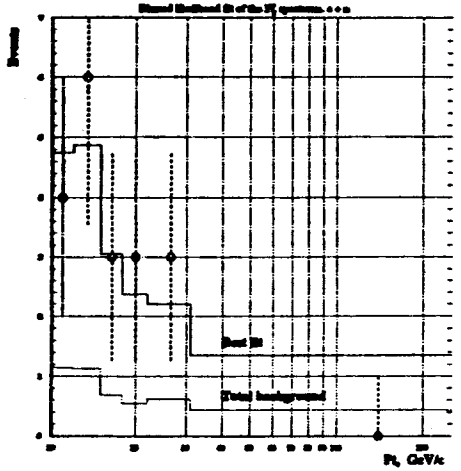

2. Experimental Results

As an example of a distribution sensitive to anomalous coupling constants, Figure 34 shows the photon transverse energy distribution for W γ events from the DØ analysis and Figure 35 the corresponding CDF data. Reasonable agreement with SM predictions is obtained in both cases and limits on the parameters $\Delta\kappa$, λ can be extracted by a statistical analysis. The resulting DØ and CDF limits are shown in Figure 36.

Because the contour limits for the two experiments are nearly identical, they lie on top of one another and are impossible to separate. The form factor scale is Λ = 1000 GeV.

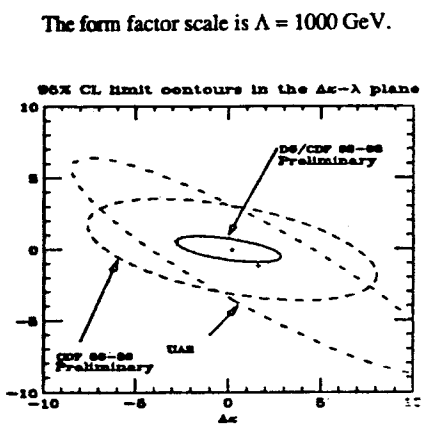

Figure 36: CDF and DØ W gamma contour plot.

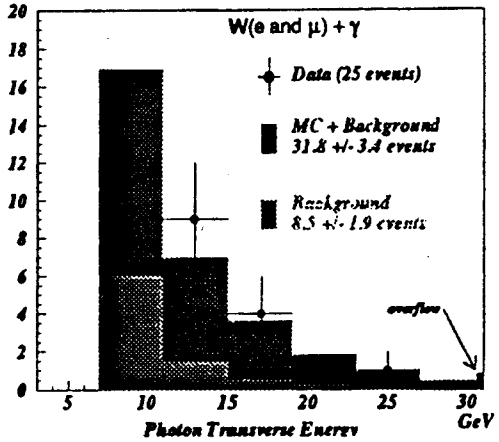

Figure 35:CDF W-gamma spectrum.

5 DØ Top Results

A. Introduction

If the top mass is greater than M_W, then it decays into W + b essentially 100% of the time, and thus, if a $t\bar{t}$ pair is produced, its decays will yield the following objects with corresponding branching ratios:

1. Dileptons—Both W's decay leptonically
   - $e\mu + \not{E}_T + 2$ b jets BR = 2.5%
   - $ee + \not{E}_T + 2$ b jets BR = 1.25%
   - $\mu\mu + \not{E}_T + 2$ b jets BR = 1.25%.
2. Single leptons + jets—Only one W decays leptonically
   - $e + \not{E}_T +$ jets BR = 15%
   - $\mu + \not{E}_T +$ jets BR = 15%
   - Decays involving τ BR = 21%.
3. All jets—Hadronic decays of the W
   - Six or more jets BR = 44%.

Although the all-jets channel has a high branching ratio, the overwhelming QCD backgrounds make this channel problematic for extracting a top signal. Potentially, the cleanest are the dilepton channels albeit with low branching ratios. Also, the lepton-plus-jets channels offer possibilities of background reduction to levels sufficient to discover top in the mass range of sensitivity. We analyze each of these latter channels in detail and extract background and signal cross sections for several assumptions about the mass of the top.

B. Dilepton Channel

The signal for these channels consists of

- two isolated leptons with high p_T,
- $\not{E}_T$, and
- hadronic jets.

The main backgrounds come from the following decay channels:

- $Z \rightarrow \text{lepton}^+ + \text{lepton}^-$,
- $W^+W^- \rightarrow \text{lepton}^+ + \text{lepton}^- + X$,
- $Z \rightarrow \tau^+ + \tau^- \rightarrow \rightarrow \text{lepton}^+ + \text{lepton}^- + X$, and
- hadrons faking leptons.

1. Electron Identification

The analysis relies on electron identification to limit backgrounds. Electrons are chosen according to the following criteria:

1. They are identified as energy clusters in the EM calorimeter.
   - They have small leakage into the hadronic calorimeter.
   - Their shower profiles are consistent with electron shapes.
   - There is a spatial match with the inner tracking chambers.
   - They are isolated.
   - The energy loss, dE/dx, in the tracking chambers is consistent with electrons.
2. They are required to lie in the pseudorapidity interval $|\eta| < 2.5$.

With these criteria, the electron detection efficiency is in the range of 45% to 80%.

2. Muon Identification

Muons are identified according to the criteria below.

There must be a track in the muon chambers. This ensures that the particle penetrated $14\lambda_0 - 18\lambda_0$ of material in the form of calorimeter and muon toroids.

1. Additional requirements:
   - Minimum ionization deposition in the calorimeter,
   - Spatial match with inner chamber track,
   - Consistency with the interaction vertex,
   - Isolation, and
   - Absence of another muon back-to-back with the candidate.
2. Pseudorapidity cut: $|\eta| < 1.7$

This results in a muon efficiency of 70% – 85%.

3. Event Selection

The event selection criteria for the three dilepton channels are summarized in Table 2 below.

Table 2: Dilepton event selection cuts.

eμ	ee	μμ
$P_t^e > 15$ GeV/c	$P_t^e > 20$ GeV/c	
$P_t^\mu > 12$ GeV/c		$P_t^\mu > 15$ GeV/c
$\not\!\!E_T > 20$ GeV		
$\not\!\!E_T > 10$ GeV	$\not\!\!E_T > 25$ GeV	
2 jets with $E_T > 15$ GeV	2 jets with $E_T > 15$ GeV	$\Delta\phi^{\mu\mu} > 140°$ if $\not\!\!E_T < 40$ GeV

The azimuthal angle requirement on the dimuon sample helps ensure that cosmic rays passing near the interaction vertex are effectively eliminated from the event sample.

Dilepton physics backgrounds come from Z and continuum Drell-Yan dilepton production, vector boson pairs (WW, WZ), and QCD production. In addition, the eμ and ee modes have a fake electron background. Only one event an eμ pair, survives all of our cuts. A plot of $1/P_T^\mu$ versus E_T^e in Figure 37 shows candidate events prior to the final jet cut. The surviving event is indicated by an * and has been described in some detail.[16] Also shown is a Monte Carlo simulation of a substantially larger run (21.3 fb^{-1}) showing where 170 GeV/c^2 top events would populate the plot. Our surviving event is at the edge of the distribution, but consistent with the expectations of the model for this top mass. The calculated background is 0.27 ± 0.09 events.

C. Electron or Muon and Jets

The signature for this decay mode is one high p_T lepton, $\not\!\!E_T$, and three or four jets. The final event selection included the use of event-shape cuts based on the aplanarity, A,[17] and another quantity, H_T, which is essentially the sum of the E_T's of the jets. The main backgrounds for the single-lepton modes are W + jets, Z + jets, and fake electrons. The e + jets fake background comes from multijet QCD events where one jet was misidentified as an electron. We estimated the fake electron background for single-electron modes from the data on the basis of the simultaneous probability for multijet

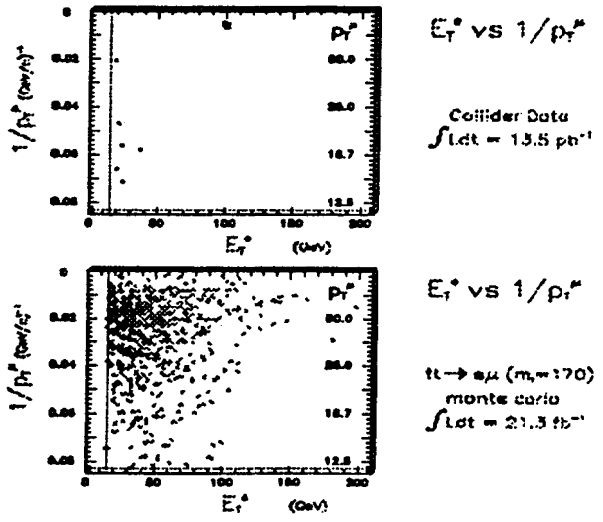

Figure 37: Muon electron plot.

QCD events to have large $\not\!\!E_T$ and for a jet to be misidentified as an electron. The W + jets background to the electron events was estimated by extrapolating the observed rate for W + 1 jet and W + 2 jet events to W + 4 or more jets. This procedure relies on the assumption that the number of jets varies as a power of α_s which has both experimental[18] and theoretical[19] support, and agrees with our data as shown in Figure 38.

For the muon sample, the W + jets background was estimated from that for electrons, since in this case neither the trigger nor the $\not\!\!E_T$ cut were efficient for one or two jets. Figure 39 shows plots of A vs. H_T for events containing e or μ and four or more jets along with corresponding plots for QCD background, background from W + jets, and a Monte Carlo generated top signal from a large exposure run. It is evident that signal to background is best in quadrant 1, where A > 0.05 and H_T > 140 GeV. The number of $t\bar{t}$ events in a quadrant is given by $N_{t\bar{t}}^i = \varepsilon_{t\bar{t}}^i \cdot f_{t\bar{t}} \cdot N$, where N is the total number of observed events with four or more jets, $\varepsilon_{t\bar{t}}^i$ is the fraction of $t\bar{t}$ expected in quadrant 1 and $f_{t\bar{t}}$ is the fraction of N that are $t\bar{t}$ events. Similarly, the corresponding background is given by $N_{bkg}^i = \varepsilon_{bkg}^i \cdot (1 - f_{t\bar{t}}) \cdot N$. Given N and the ε's, we can fit for top using Poisson statistics. The results of the fit give $f_{t\bar{t}} = 0.27 \pm 0.25$ for the fraction of events in the sample with four or more jets. The number of observed events is 4, 1, 4, and 5 in quadrants 1 to 4 while the predicted numbers are 4.3, 3.0, 2.7, and 4.1. There is a large systematic error (35%) from the choice of partitioning the A, H_T plane and a 20% systematic error from the uncertainty in calculating the fractions in each quadrant. The number of $t\bar{t}$ events in this sample is thus $N_{t\bar{t}} = 3.6 \pm 3.3(\text{stat.}) \pm 1.5(\text{sys.})$ which leads to a cross section of $\sigma_{t\bar{t}} = 7.4 \pm 6.9$ (stat.) $\pm$ 3.6 (sys.) pb. In a separate analysis, we show that these numbers are consistent with top production and W + jets backgrounds estimated from scaling.

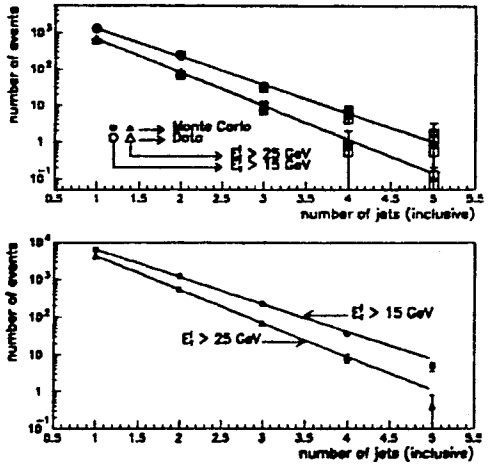

Figure 38: W + jets plots.

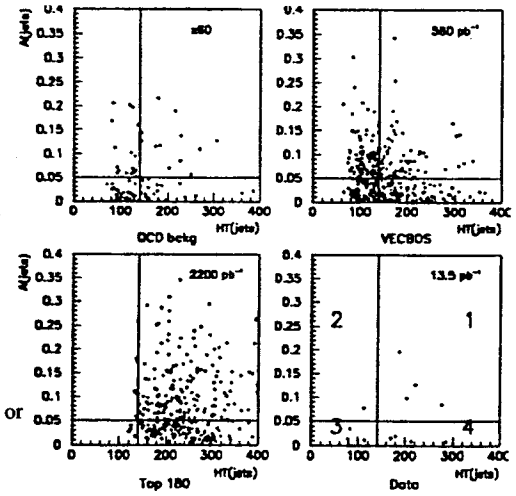

Figure 39: Aplanarity vs. HT plot.

D. *Electron and Jets and Mutag*

Since the top decay cascade t-->b-->c-->s--> d has a high probability of producing a lepton from a semileptonic decay, detecting the presence of such a "tag" is a powerful tool for improving the signal-to-noise ratio. In our case, we use a μ tag because of the relative ease of its identification and measurement. Approximately 44% of $t\bar{t}$ events contain a soft muon associated with a b jet. In about 20% of $t\bar{t}$ events, the soft muon will be detected with the cuts used in this analysis.

The basic cuts in this analysis include:

- selection of a tight electron with E_T>20 GeV and $|\eta_{det}|$<2.0,
- three jets with E_T>20 GeV and $|\eta|$<2.0,
- $\not\!\!E_T$ >20 GeV, and
- a muon with p_T>4.0 GeV and $|\eta_{det}|$<1.7. If p_T>12 GeV, μ is required to be non-isolated.

With these selections, 34 events survive all cuts before the μ tag is imposed. After all cuts two events remain.

1. Backgrounds

There are two major sources of backgrounds in this channel: W + jets with a muon, either fake or real, and "fake events" in which QCD multi-jet events fake a signal event. Both sources of backgrounds are estimated from the data. We attempt to

calculate backgrounds without muons and then use the measured rates per jet to estimate the final backgrounds.

a) W + Jets + μ Tag Background

We start with a sample of events from our inclusive electron trigger which contains predominantly fake events. It may have a different jet E_T distribution than our desired W + jets events and the heavy quark content could be different. We therefore compute the muon rate per jet as a function of the jet E_T. We check this rate against a QCD dijet sample (Figure 40 shows the good agreement in muon P_t and radial distribution relative to jet axis), direct photons, and a sample of multijet data. We apply the measured rate to the 34 events in the sample before the muon tag and get a background of 0.43±0.14 events.

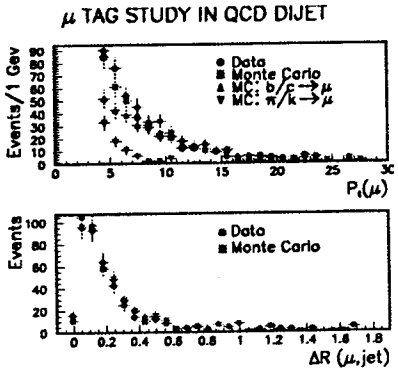

Figure 40: Muon P_T and ΔR in QCD dijets.

b) Fake Event Background

Starting once again with a sample of inclusive electron trigger events, we divide them into two samples:

1. Events satisfying standard tight electron criteria.
2. Events that contain an object with EM fraction > 90% but fail the tight electron cuts. These are called "bad electrons."

Using the $\mathbf{E}_T$ distributions of the two samples, calculate the fake background with muon tag. The yield is 6.3 ± 1.7 events as background to our sample of 34 W(ev) events. We next use the "bad electron" sample to deduce the muon rate per jet as a function of $\mathbf{E}_T$. This measured rate is then applied to the background before muon tag to get the final background estimate from fake events: 0.12 ± 0.05 events.

c) Background Checks

Using events that contain no top, we can check our background estimates. We use a sample containing one loose electron, missing E_T > 20 GeV, one jet, and a muon tag. We vary the jet threshold and estimate the number of events expected from W + jets and from fakes using the same cuts as before. Good agreement between observation and prediction is obtained.

2. Summary of Results of e + Jets + μ Tag

The signal and background for this channel is summarized in Table 3. Also shown are the expected number of signal events for three choices of the top mass.

E. Summary and Prospects

We may combine all the channels analyzed above to extract a top cross section and associated uncertainty. Doing this, we obtain seven events with a background of 3.2 ± 1.1 events. The probability that our background fluctuated to give this signal is 7.2%. We obtain a cross section of 7.2 ± 5.4 pb at a top mass of 160 GeV/c^2. Since the acceptance varies with the mass of top, the central values and uncertainties are both a function of this mass. Figure 41 is a plot of the theoretical prediction[20] for the top cross section with both the CDF and DØ measurements superimposed. The theoretical prediction is displayed as a band to reflect its inherent uncertainties. Clearly, within statistics, the DØ and CDF results are compatible and the DØ result by itself is consistent with no top production.

Table 3: Summary of e + jets + mu tag.

Category	Events
Data	2
Background	
W + jets	0.43 ± 0.14
Fake events	0.12 ± 0.05
Total	0.55 ± 0.15
Expected Events	
M(top) =140	1.3 ± 0.4
M(top)=160	1.0 ± 0.2
M(top)=180	0.6 ± 0.2

The details of our analysis are further summarized in Table 4 below. Tabulated are the efficiency x branching ratio and the number of expected top events as a function of top mass for all channels reported, the number of observed events, and the estimated number of background events for each channel and whether that channel was included in previously published results from DØ.

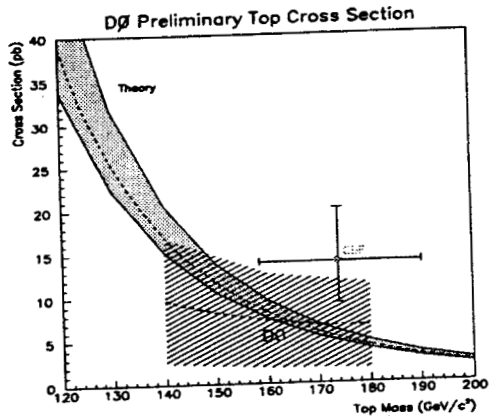

Figure 41: Top cross section prediction with DØ and CDF data .

This paper summarizes the situation as it was in August 1994. Since then, a paper summarizing the results of the DØ top search in data taken during the 1992-93 run has been submitted for publication in the *Physical Review Letters*.

Table 4: Summary of final results for all channels.

M(GeV/c²)	eμ	ee	μμ	e + jets	μ + jets	e + jets (μ)	All
New?	No	No	Yes	No	No	Yes	
εxBR(%) 140	0.32±0.06	0.18±0.02	0.11±0.02	1.2±0.3	0.8±0.2	0.6±0.2	
$\langle N_s \rangle$ 140	0.72±0.16	0.41±0.07	0.24±0.05	2.8±0.7	1.3±0.4	1.3±0.4	6.7±1.2
εxBR(%) 160	o.36±0.07	0.20±0.03	0.11±0.01	1.6±0.4	1.1±0.3	0.9±0.2	
$\langle N_s \rangle$ 160	0.40±0.09	0.22±0.04	0.12±0.02	1.8±0.5	0.9±0.3	1.0±0.2	4.4±0.7
εxBR(%) 180	0.41±0.07	0.21±0.03	0.11±0.01	1.7±0.4	1.2±0.3	1.1±0.2	
$\langle N_s \rangle$ 180	0.23±0.05	0.12±0.02	0.06±0.01	1.0±0.2	0.5±0.2	0.6±0.2	2.5±0.4
Bkgrnd.	0.27±0.09	0.16±0.07	0.33±0.06	1.2±0.7	0.6±0.5	0.6±0.2	3.2±1.1
$\int$Ldt (pb^{-1})	13.5±1.6	13.5±1.6	9.8±1.2	13.5±1.6	9.8±1.2	13.5±1.6	
Data	1	0	0	2	2	2	7

VI. Conclusions

The 1992-93 run analyses have contributed much to our current understanding of collider physics and they offer tantalizing glimpses of new possibilities in the future when higher luminosities will become available. We have learned much already about QCD phenomena including jet shapes, jet production, and the production of direct photons. Possible disagreements with predictions based on current structure functions are suggestive. In the electroweak sector, the M_W measurements are making good progress and there is every expectation that substantial improvements are possible with more luminosity. There are new and interesting limits on anomalous couplings and in the area of new phenomena, the possible phase space is substantially reduced. The situation in the top sector is dissatisfying at the present time as there is not sufficient evidence to claim discovery. It is here, perhaps, that we anticipate the biggest breakthroughs in the coming years with higher luminosities. If the top mass is indeed around 174 GeV as suggested by the CDF data, then by the end of this decade, it will be firmly established and its mass will be measured with good precision.

[1] The underlying event has been determined to contribute a constant transverse energy density of 0.55 GeV per unit area in η, ϕ space.

[2] Uranium noise contributes a constant energy density of 1.36 GeV in η, ϕ space.

[3] R. Brun et al., "GEANT Users Guide," CERN Program Library.

[4] F. Paige and S. Protopopescu, ISAJET v6.49 Users Guide, BNL Report No. BNL38034, 1986 (unpublished).

[5] G. Marchesini and B. R. Webber, Nucl. Phys.B **310**, 461 (1988).

[6] H. U. Bengtsson and T. Sjostrand, Computer Phys. Comm. **46**, 43 (1987).

[7] W. T. Giele, E. W. N. Glover, and D. A. Kosower, Nucl. Phys.B **403**, 93 (1993).

[8] A study of the differences between quark and gluon jets using vertex tagging of quark jets. OPAL Collaboration, CERN-PPE/93-02 (1993).

[9] CDF Collaboration, F. Abe et al., Phys. Lett. **68**, 1104 (1992).

[10] UA-2 Collaboration, J. A. Appel et al., Phys. Lett. **160B**, 349 (1985).

[11] G. Cocconi, Phys. Rev. **111**, 1699 (1958).

[12] M. L. Good and W. D. Walker, Phys. Rev. **120**, 1857 (1960).

[13] Y. Dokshitzer, V. Khoze, and S. Troyan in *Physics in Collision VI*, Proceedings of the International Conference, Chicago, IL, 1986, edited by M. Derrick. (World Scientific, Singapore, 1987) p. 365.

[14] J. D. Bjorken, Phys. Rev. D 47, 101 (1993).

[15] CDF Collaboration: F. Abe et al., Phys. Rev. Lett. **73**, 94 (1994), F. Abe et al., Phys. Rev. D **50**, 2966 (1994).

[16] DØ Collaboration, S. Abachi et al., Phys. Rev. Lett. **72**, 2138 (1994).

[17] The aplanarity is defined as 3/2 times the largest eigenvalue of the transverse momentum tensor normalized to unit trace.

[18] F. Abe et al., Phys. Rev. Lett. **70**, 4042 (1993).

[19] F. Behrends, H. Kuijf, B. Tausk, and W. Giele, Nucl. Phys.B **357**, 32 (1991).

[20] E. Laenen, J. Smith, and W. van Neerven, Phys. Lett. **321B**, 94 (1994).